


Holocene climate history of the Nunatsiavut (northern Labrador, Canada) established from pollen and dinoflagellate cyst assemblages covering the past 7000 years

The Holocene
2016, Vol. 26(1) 44–60
© The Author(s) 2015
Reprints and permissions:
sagepub.co.uk/journalsPermissions.nav
DOI: 10.1177/0959683615596823
hol.sagepub.com


Thomas Richerol,¹ Bianca Fréchette,² André Rochon³
and Reinhard Pienitz¹

Abstract

This study documents the past ~7000 years of Holocene climatic history for Labrador and Nunatsiavut, using a sedimentary sequence of more than 8 m retrieved in Nachvak fjord, one of the northernmost fjords of Nunatsiavut. Using a multi-proxy approach combining a solid Accelerator Mass Spectrometry (AMS)-¹⁴C chronology and the fossil assemblages of pollen grains and dinoflagellate cysts (dinocysts), we were able to compare terrestrial and marine records in an effort to obtain a better understanding of the mid- to late-Holocene climate history of the Nunatsiavut. Records begin at the end of the deglaciation and showed a general delay in the sequence of climate events which followed, both in terrestrial and marine realms. The presence of *Pentaparsodinium dalei* in great abundance in Nachvak Fjord revealed a strong influence of the North Atlantic Ocean and the Labrador Sea until ~3000 yr BP. Afterward, its rather fast disappearance marked the increased influence of Arctic waters. The last 1000 years show climate stability in the region over the marine realm and a cooling trend over terrestrial landscapes.

Keywords

dinocysts, fjord, Holocene, Nunatsiavut, paleoclimate, palynology

Received 25 November 2014; revised manuscript accepted 27 May 2015

Introduction

The climate history of the Holocene has been well documented in the Arctic, Sub-Arctic, west and south Greenland, and Newfoundland (Carlson et al., 2007; Kaplan and Wolfe, 2006; Kaufman et al., 2004; Kerwin et al., 2004; Macpherson, 1982; Marcott et al., 2013; Renssen et al., 2009; Ritchie, 1987). Labrador is the continental part of the province known as 'Newfoundland and Labrador' on the northeastern Atlantic coast of Canada. Our study region is located in the northern part of the province, also called Nunatsiavut, which belongs to the native Labradorian Inuit.

Nunatsiavut and Labrador in general have been known to be stable in terms of climate throughout the Industrial Era (IE), with no evidence of fluctuations associated with the recent human-induced climate changes and the warming observed in most other Arctic and Sub-Arctic regions (Arctic Climate Impact Assessment (ACIA), 2005; Arctic Monitoring and Assessment Programme (AMAP), 2011; Barber, 2010; Intergovernmental Panel on Climate Change (IPCC), 2013–2014; Reimer and Biasutti, 2012; Richerol et al., 2014; Sheldon and Bell, 2012, 2013; Smol et al., 2005). During the last glaciation (Wisconsinan: ~80,000 to 11,000 BP), the Laurentide Ice Sheet covered the entire region. A warming period called the Holocene Thermal Maximum (HTM) occurred ~11,000–6000 BP (Gibbard et al., 2010; Johnson et al., 1997; Karrow et al., 2000; Syverson and Colgan, 2011). However, depending on the deglaciation pattern of the Laurentide Ice Sheet and the influence of orbital cycles, the timing and magnitude of the warming varied substantially between western and eastern Canada (Renssen et al., 2009). An abrupt deglaciation of

the central part of the Laurentide Ice Sheet over Hudson Bay occurred between 9000 and 8400 BP because of glacial outburst flood events through Hudson Strait (Barber et al., 1999; Carlson et al., 2007; Dyke, 2004; Lajeunesse and St-Onge, 2008). Paleoclimate records show a delayed onset of the HTM between 7000 and 6000 BP over central and northeastern North America and southern Greenland (Carlson et al., 2007; Kaplan and Wolfe, 2006; Kaufman et al., 2004).

In Newfoundland (South of Labrador), the deglaciation began around 10,000 BP and palynological records reveal that vegetation re-colonized the area after 9300 BP (Bell et al., 2005b; Macpherson, 1982; Ritchie, 1987; Shaw et al., 2002, 2006), allowing first human occupations around the same period (Bell

¹Aquatic Paleoecology Laboratory, Centre d'Études Nordiques and Department of Geography, Université Laval, Canada

²Centre de recherche en géochimie et en géodynamique (Geotop), Université du Québec à Montréal, Canada

³Laboratoire de Palynologie Marine, Institut des Sciences de la Mer (ISMER), Université du Québec à Rimouski, Canada

Corresponding author:

Thomas Richerol, Laboratoire de Paléocéologie Aquatique, Centre d'Études Nordiques and Department of Geography, Université Laval, 2405 Rue de la Terrasse, Pavillon Abitibi-Price, Québec, QC G1V 0A6, Canada.

Email: thomas_richerol@yahoo.fr

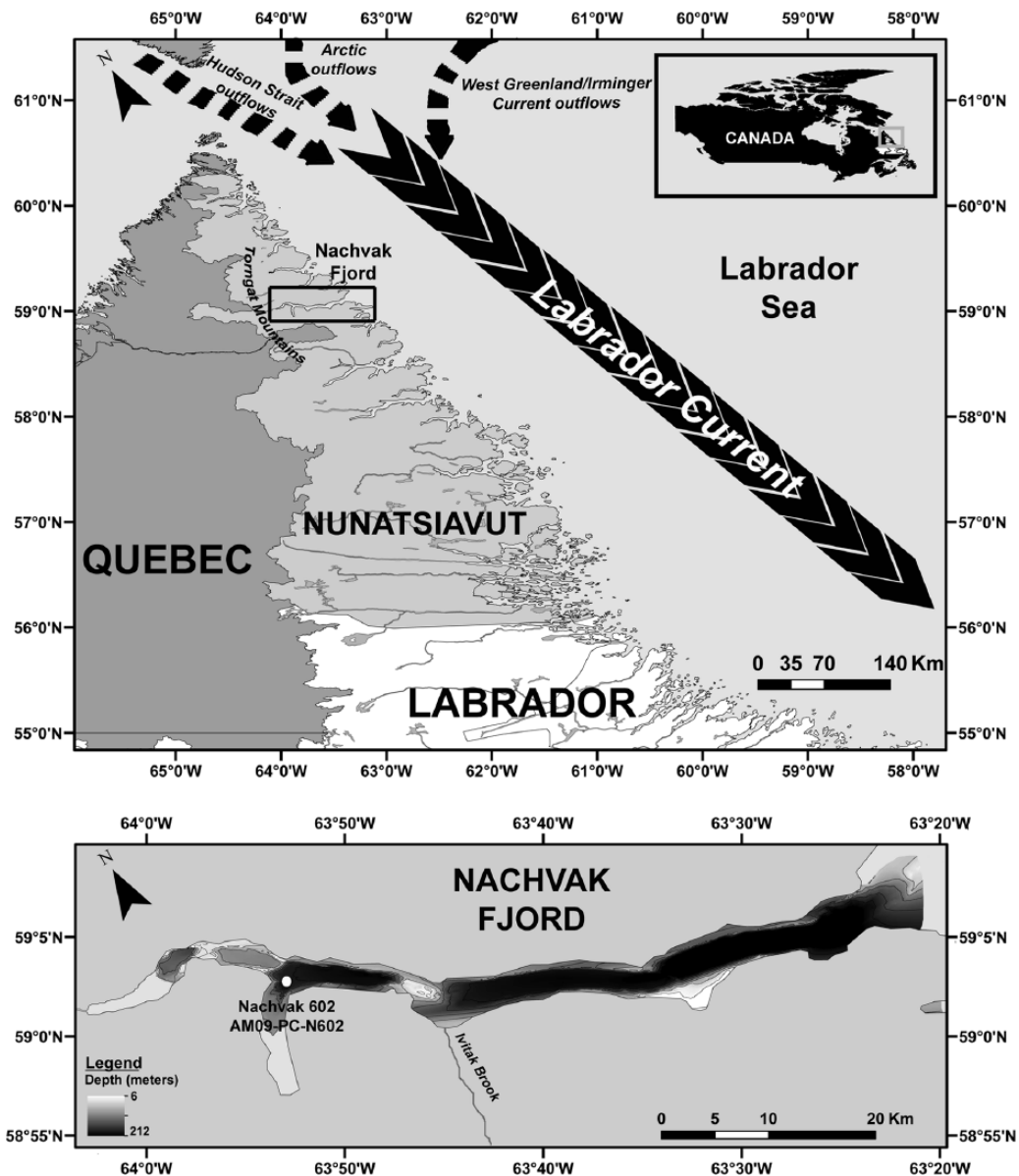


Figure 1. Map of the Nunatsiavut (North Labrador, Canada) illustrating the location of the piston core retrieved from Nachvak fjord (modified from Richerol et al., 2012).

et al., 2005a; Bell and Renouf, 2003). A paleolimnological study of lakes from Nova Scotia and Newfoundland recorded the maximum of this warming period between ~6300 and 4200 BP (McCarthy et al., 1995). Further North, around 7000 BP, the conditions were cooler over regions directly influenced by the presence of the remnants of the Laurentide Ice Sheet (Bell et al., 2005a, 2005b; Bell and Renouf, 2003; Renssen et al., 2009). Previous studies suggested its disappearance around 7000 BP, with the persistence of some small ice caps in northern Québec and Labrador until 6000 BP (Carlson et al., 2008; Peltier, 2004; Renssen et al., 2009; Saulnier-Talbot and Pienitz, 2010), delaying the recolonization by vegetation in Labrador to ~5500–5000 BP (Lamb, 1984, 1985).

This study represents the first step in documenting the transitional period between the last glaciation and the IE for Labrador and Nunatsiavut. In 2009, a sedimentary sequence of more than 8m was retrieved in Nachvak fjord, one of the northernmost fjords of Nunatsiavut (Figure 1). Our objectives were to use a multi-proxy approach in order to reconstruct part of the Holocene climate history within Nunatsiavut. Such study will provide useful information about the

Holocene climate history of a poorly known Sub-Arctic region, thus strengthening the climate change models for the Canadian Arctic. Combining a solid Accelerator Mass Spectrometry (AMS)-¹⁴C chronology and the fossil assemblages of pollen and dinocysts, we were able to compare the terrestrial and marine records in an effort to obtain a better understanding of the mid- to late-Holocene climate history of the Nunatsiavut, from the beginning of interglacial conditions ~7000 years ago until the present day.

Study region

Labrador extends between 50°N and 60°N, along the Labrador Sea, and lies on Precambrian rocks from the Canadian Shield (De Blij, 2005). Most of the region is elevated, between 450–750 m.a.s.l. In the North-East, near the border with the province of Québec, the Torngat Mountains range rises up to 1600 m.a.s.l. (Short and Nichols, 1977) (Figure 1).

Western and Central Labrador are characterized by broad flat till plains covered by extensive peatlands and large shallow lakes. To the North, the coastal landscape is dominated by hills dissected

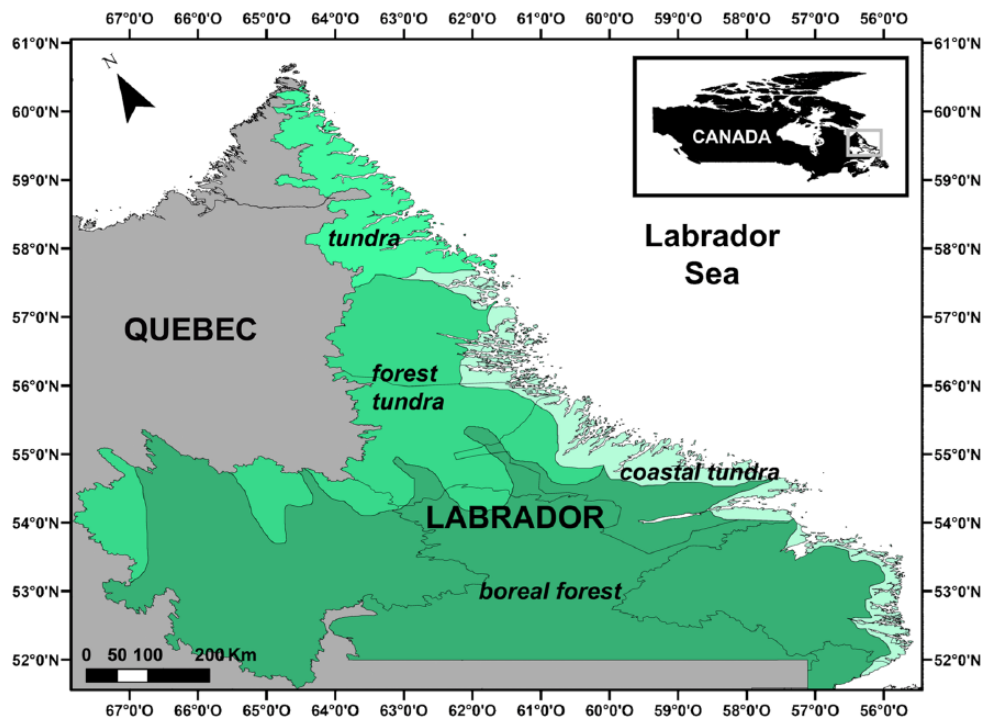


Figure 2. Map of the four biogeographical zones of Labrador vegetation.

by large rivers and majestic fjords (Engstrom and Hansen, 1985). These fjords are influenced by both Atlantic and Arctic water masses and receive freshwater, nutrients, and sediments from glaciers and rivers. The northernmost fjords are typically long, narrow inlets carved by glacier ice, with deep muddy basins separated by rock sills and flanked by tall, steep sidewalls. In contrast, central Labrador fjords, though also of glacial origin, are shallow, irregularly shaped inlets with gently sloping sidewalls and large intertidal zones (Brown et al., 2012). The surface stratification in the fjords is controlled by both runoff and ice melt. During summer, a strong pycnocline with fresh surface waters overlies more saline intermediate waters and is more pronounced in the northern fjords, whereas during the fall, the water column is more homogeneous (non-stratified). Circulation appears to occur at all depths, as the waters in the fjords are oxygen-rich. Nutrient distributions in the fall (surface and bottom) reveal a pattern of nitrate and phosphate depletion from the northernmost to the southernmost fjords (Brown et al., 2012; Richerol et al., 2012).

The climate of Labrador is characterized by long cold winters and cool moist summers. The temperature and moisture regimes are dominated by north-south transgressions of cold dry Arctic air and warm moist Atlantic air (Hare and Hay, 1974). The climate of Labrador is significantly influenced by the cold Labrador Current (Figure 1), resulting in a strong climatic contrast between the coastal and inland Labrador (Engstrom and Hansen, 1985). In summer, the mean temperature on the coast is 10°C, while it can reach 16–38°C inland. In winter, the mean temperature on the coast is –12°C, relatively 3°C warmer than inland on average (De Blij, 2005; Short and Nichols, 1977; Ullah et al., 1992). In the last decade, the Labrador fjords have been frozen from the second half of December to the first half of July (Richerol et al., 2012). Mean annual precipitation, which is divided equally between summer and winter, varies between 750 mm in the North and 960 mm in the South. Snowfalls are relatively important with annual quantities ranging between 390 and 480 cm (De Blij, 2005; Ullah et al., 1992).

The vegetation of Labrador can be divided into four biogeographical zones along a North-South gradient (Jessen et al., 2011; Lamb, 1984; Williams et al., 2000): tundra, forest tundra, coastal

tundra, and boreal forest (Figure 2). South of 56°N, except for the entire coastal fringe where tundra vegetation is found because of a severe oceanic climate, Labrador is covered by boreal forest (Figure 2). This is a continuous dense forest with a moss-rich land cover. The black spruce (*Picea mariana*) is dominant, accompanied by some balsam poplar (*Populus balsamifera*), white poplar (*Populus tremuloides*), white birch (*Betula papyrifera*), mountain ash (*Sorbus decora*), and alder (*Alnus* sp.) (Jessen et al., 2011; Richard, 1995; Williams et al., 2000). North of 56°N, Nunatsiavut is a landscape of forest tundra and tundra (Figures 1 and 2). In the forest tundra, the most common tree species is black spruce along with some white spruce (*Picea glauca*) and eastern larch (*Larix laricina*). The tundra is mostly composed of dwarf shrubs (*B. papyrifera*, *Betula glandulosa*, *Alnus crispa*, and *Salix* sp.), graminoids, herbs, mosses, and lichens (Fallu et al., 2002; Lamb, 1984, 1985; Roberts et al., 2006).

Nachvak is the northernmost fjord of the region, located in the Torngat Mountains National Park Reserve, hence it is a remote and pristine tundra ecosystem (Figure 1) (Brown et al., 2012). Nachvak Fjord is a 45 km-long glacial trough in the Torngat Mountains, with steep sidewalls rising to 1 km from sea level and a deep basin down to 200 m depth. The fjord is 2–4 km wide, widening gradually eastward to Nachvak Bay which opens to the Labrador Sea (Bell and Josenhans, 1997). From the head to the mouth of the fjord, the depth of the basins increases from 90 m to 210 m. The basins are separated by sills present between 10 and 180 m a.s.l. and composed of either rock materials or glacial deposits (Bell and Josenhans, 1997). Nachvak Fjord receives most of its sediment from Ivitak Brook, a glaciated catchment (Bentley and Kahlmeyer, 2012; Kahlmeyer, 2009).

Methodology

Sampling

Sampling in Nachvak fjord was carried out in November 2009 during leg4b of the *ArcticNet* campaign onboard the Canadian Coast Guard Ship *Amundsen*. A sedimentary sequence (812 cm) was collected at station 602 (59.5265°N, 63.8784°W) using a

Table 1. Table detailing the statistical data associated with the calibration of the AMS-¹⁴C dates obtained throughout the core.

University of California #	Laval University #	Mean core depth (cm)	¹⁴ C age	95.4% (2σ) calibrated age ranges (cal. BP)	Relative area under distribution	cal. BP ^a	Calibration data
UCIAMS-76371	ULA-1587	92.5	1505 ± 15	781–996	1.000	890 ± 108	Reimer et al. (2013)
UCIAMS-76372	ULA-1588	148.5	2120 ± 15	1398–1646	1.000	1520 ± 124	
UCIAMS-76376	ULA-1592	212.5	2725 ± 20	2125–2341	1.000	2230 ± 108	
UCIAMS-76378	ULA-1594	347.5	3735 ± 15	3367–3586	1.000	3480 ± 110	
UCIAMS-76379	ULA-1595	407.5	4075 ± 15	3790–4062	1.000	3930 ± 136	
UCIAMS-76380	ULA-1596	411.5	4075 ± 20	3780–4062	1.000	3920 ± 141	
UCIAMS-76381	ULA-1597	433.5	4210 ± 15	3954–4232	1.000	4090 ± 139	
UCIAMS-76384	ULA-1600	444.5	4250 ± 15	3989–4289	1.000	4140 ± 150	
UCIAMS-76386	ULA-1602	448.5	4320 ± 15	4118–4393	1.000	4260 ± 138	
UCIAMS-76385	ULA-1601	458.5	4340 ± 15	4144–4403	1.000	4270 ± 130	
UCIAMS-76389	ULA-1605	464.5	4415 ± 20	4236–4505	1.000	4370 ± 135	
UCIAMS-76388	ULA-1604	473.5	4520 ± 15	4395–4653	0.992	4520 ± 129	
				4664–4675	0.008		
UCIAMS-76387	ULA-1603	494.5	4700 ± 20	4605–4851	1.000	4730 ± 123	
UCIAMS-76391	ULA-1607	520.5	4865 ± 15	4825–5078	0.993	4950 ± 127	
				5100–5110	0.007		
UCIAMS-76390	ULA-1606	556.5	5195 ± 15	5292–5517	1.000	5400 ± 113	
UCIAMS-76394	ULA-1610	630.5	5590 ± 20	5697–5913	1.000	5800 ± 108	
UCIAMS-76393	ULA-1609	636.5	5580 ± 15	5692–5904	1.000	5800 ± 106	
UCIAMS-76392	ULA-1608	647.5	5620 ± 20	5720–5943	1.000	5830 ± 112	
UCIAMS-78279	ULA-1746	804.5	6550 ± 15	6749–6993	1.000	6870 ± 122	
UCIAMS-78280	ULA-1747	810.5	6545 ± 15	6744–6987	1.000	6870 ± 122	

AMS: Accelerator Mass Spectrometry.

^aThe authors of the Calib 7.0 software (Reimer et al., 2004, 2013) recommend to round the calibrated age ranges to the nearest 10 years for samples with standard deviations (±error in the age) greater than 50 years.

piston corer triggered by a gravity corer. This piston core was cut into eight sections of approximately 100 cm each for easiest storage and transport. The eight sections were described and sampled at the Laboratory of Marine Palynology, Institut des sciences de la mer, Université du Québec à Rimouski (ISMER-UQAR), in Rimouski (Québec). The geophysical analyses (density, magnetic susceptibility) were performed at 0.5 cm intervals for each section. The percentages of organic matter and water content were measured every 1 cm. The grain-size and microfossil analyses (dinocysts, pollen and spores, *Halodinium* sp., foraminifer linings, and pre-Quaternary palynomorphs) were performed at 10 cm intervals for each section in the Aquatic Paleoecology Laboratory (APL – Laval University, Québec City). The palynological analyses were performed using the standard method described in Rochon et al. (1999) and Richerol et al. (2008a, 2008b, 2012).

Stratigraphic analysis

Grain-size analysis. The particle-size composition of the core was determined at 10 cm intervals using the laser granulometer Horiba® LA950v2. The samples were prepared following the protocol from the Laboratory of Geomorphology and Sedimentology at Laval University (Québec, QC). The free software Gradistat v4 (Blott and Pye, 2001) was used to statistically separate the different grain sizes and their percentages, as well as calculate standard statistical parameters (mean, median, and sorting) using the mathematical ‘method of moments’ (Krumbein and Pettijohn, 1938).

Multi-sensor core logger. Low-field volumetric magnetic susceptibility (K), density (d), and fractional porosity (FP) were measured at the Sedimentary Paleomagnetism and Marine Geology Laboratory of ISMER-UQAR (Rimouski, QC) using a GEOTEK™ multi-sensor core logger (MSCL) at 0.5 cm intervals for each core.

The volumetric magnetic susceptibility (K) is a dimensionless parameter measuring the magnetization of a volume induced by applying a magnetic field to a material. It is used for marine sediments because variations in density in sediment cores are relatively small (Gunn and Best, 1998). Because of the near zero magnetic susceptibility of the pore-water, the porosity can have an impact on the volumetric magnetic susceptibility by diluting the amount of magnetic carrier mineral in the core and thus underestimating the total magnetic susceptibility. We therefore quantified this effect (Kp) by assuming zero susceptibility for the pore volume (Niessen et al., 1998):

$$Kp = \frac{K}{(1 - FP)} \quad (1)$$

Chronological framework

A chronology was established based on 20 AMS-¹⁴C ages obtained from shell fragments found at various depths throughout the core. The identification of the species of shell is very difficult because of the degree of fragmentation. However, based on previous shells found in a core taken in Saglek Fjord (Richerol et al., 2014), the fragments are likely to be from *Macoma baltica* and/or *Littorina littorea* (pers. comm.). The preparation of the samples was performed at the Radiochronology Laboratory of the Center for Northern Studies (Laval University, Québec City, Canada) and the analyses at the Keck Carbon Cycle AMS Facility (Earth System Science Department, University of California at Irvine, USA). The calibration of conventional AMS-¹⁴C dates into cal. BP dates was done using the software CALIB 7.0 online (Stuiver et al., 2005) and MARINE13 (Reimer et al., 2013). The station 899 in Komaktorvik Fjord (Labrador: 59.28°N, –63.73°W), being the nearest to our coring site, was chosen to estimate a value for marine reservoir corrections ($\Delta R = 150 \pm 40$) (Table 1).

Table 2. Table summarizing the information of the parameters reconstructed from fossil pollen and dinocyst assemblages (from Richerol et al., 2014): parameter denomination and codename, unit, correlation coefficient (R^2), and Root Mean Square Error (RMSE) of the validation.

Parameter	Unit	R^2	\pm RMSE
Pollen-based paleoclimatic reconstructions			
Total annual precipitation	mm	0.81	210.35
Mean temperature of the coldest month of the year	$^{\circ}\text{C}$	0.92	3.26
Mean temperature of the warmest month of the year	$^{\circ}\text{C}$	0.91	1.67
Dinocyst-based paleoceanographic reconstructions (Richerol et al., 2014)			
Sea-surface temperature of August	$^{\circ}\text{C}$	0.95	1.72
Sea-surface salinity of August	psu	0.72	2.22
Sea-ice cover duration	months yr^{-1}	0.86	1.33
Annual productivity	$\text{g C m}^{-2}\text{yr}^{-1}$	0.80	61.27

Palynological preparation

Fossil palynomorph preparation (pollen, spores, dinocysts, acritarchs, freshwater and pre-Quaternary palynomorphs) followed standard procedures as outlined in Richerol et al. (2008a, 2008b, 2012). Concentration of the palynomorphs (specimens cm^{-3}) was calculated using the known concentration ($12,100 \pm 1892$ spores by tablet, batch #414831) of the *Lycopodium* sp. spores tablet introduced during the preparation (Mertens et al., 2009; Richerol et al., 2012).

In addition to the dinocysts, which are good indicators of planktonic productivity (Richerol et al., 2008b), we have identified and counted four other types of palynomorphs:

- *Halodinium* sp., an acritarch and freshwater tracer (Richerol et al., 2008b);
- Terrestrial palynomorphs such as pollen grains and spores, which allow vegetation and terrestrial climate to be compared with oceanographic change (Richerol et al., 2008b);
- Foraminifer linings, indicators of benthic marine productivity (De Vernal et al., 1992);
- Pre-Quaternary palynomorphs (reworked palynomorphs), including dinocysts, acritarchs, pollen grains and spores, which are indicators of inputs of ancient and/or distant erosive material (De Vernal and Hillaire-Marcel, 1987; Durantou et al., 2012).

Palynomorphs were counted using a transmitted-light microscope (Leica DM5500B) with a magnification factor of $400\times$ at APL (UL, Québec City). A minimum of 300 dinocysts were counted in each sample before stopping the counting of all palynomorphs. This method yields the best statistical representation of all the taxa present in the samples. The nomenclature used for the identification of the dinocysts corresponds to Rochon et al. (1999), Head et al. (2001), the index of Lentin and Williams (Fensome and Williams, 2004) and Radi et al. (2013). The identification of the pollen and spores was performed using the Laurentian flora of Frère Marie-Victorin (1935) as well as Rousseau (1974), to account for the species encountered in Nunatsiavut, and McAndrews et al. (1973) for the pollen and spore micrographs.

Studies from Zonneveld et al. (1997, 2001) and Zonneveld and Brummer (2000) have shown species sensitivity to oxygen availability. The cysts from the *Protoperidinium* group, such as *Brigantedinium* sp., are the most sensitive, followed by the genera *Spiniferites*, *Impagidinium*, and *Operculodinium*. A recent study by Bogus et al. (2014) revealed a difference in composition of the dinosporin forming the wall of the cyst, depending on the nutritional behavior of the related dinoflagellate. Phototrophic dinoflagellates may produce more resistant cysts than heterotrophic dinoflagellates. The high sedimentation rates measured in the Nunatsiavut fjords helped preserving dinocyst assemblages from oxidation (Richerol et al., 2014), and the most sensitive taxa, such

as *Brigantedinium* sp., showed excellent preservation, with the operculum still attached on many specimens. Moreover, the everlasting presence of more oxygen-sensitive cysts from heterotrophic dinoflagellates in sediments from Nunatsiavut's fjords provides solid evidence of a well-preserved record.

Statistical analyses

Biozonations through clustering. In order to statistically distinguish the major changes in the dinocyst and pollen assemblages, we used the R software in combination with the libraries 'vegan' and 'rioja' to produce a cluster showing the Euclidean distance between each sample for each core. Using the 'decostand' function, our relative abundance data have first been standardized prior to the transformation of the resultant data matrix to a Euclidean distance matrix. The grouping test CONISS was then applied to the distance matrix using the 'chclust' function (Borcard et al., 2011). For each core section, a graphical stratigraphically constrained clustering has been obtained according to time.

Pollen-based quantitative paleoclimatic reconstructions. The reconstructions of terrestrial environmental parameters were performed with the software 'R' and the reconstruction technique of the modern analog (RecMAT). The modern pollen assemblage database includes ' $N=4833$ ' sites from lakes, peats, moss cushions, and other terrestrial deposits of North America and Greenland, distributed among 10 vegetation types (biomes) (Whitmore et al., 2005). The methodology applied has been described by Fréchet et al. (2008). We have chosen to group together the Asteraceae because of an inability to distinguish between different species. This database includes 69 climatic and bioclimatic parameters. The following were reconstructed and results were compared with the dinocyst-based paleoceanographic reconstructions: mean monthly temperature ($^{\circ}\text{C}$) and precipitation (mm) for each month, total annual precipitation (mm), and mean temperature of the coldest and warmest month ($^{\circ}\text{C}$). The climate estimates were calculated from the five best modern analogs. The validation of the database provided strong correlation coefficients and a Root Mean Square Error (RMSE) for each reconstructed parameter (Table 2).

Dinocyst-based quantitative paleoceanographic reconstructions. The reconstructions of sea-surface parameters (August sea-surface temperature ($^{\circ}\text{C}$) and salinity (psu), sea-ice cover duration (months yr^{-1}) and annual productivity ($\text{g C m}^{-2}\text{yr}^{-1}$)) were performed with the software 'R' using fossil dinocyst assemblages, transfer functions, and the search of five analogs in the GEOTOP modern dinocyst database ($N=1441$) (Richerol et al., 2008b, 2014). Here, we also used the 'bioindic' package developed on the R-platform (<http://cran.r-project.org/>), which is specially designed to offer various types of statistical analyses.

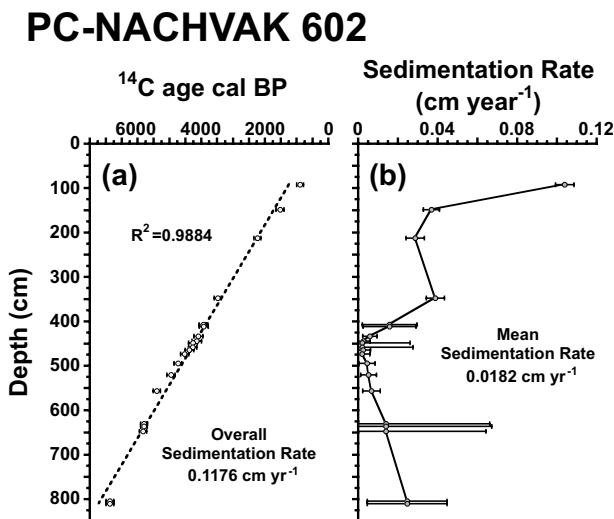


Figure 3. Age–depth model based on the AMS- ^{14}C chronology from the piston core representing (a) each ^{14}C age cal. BP according to core depth (cm) and (b) the estimated rate of sediment accumulation (cm yr^{-1}) at each dated depth in the core.

Results

Chronological framework

The 20 AMS- ^{14}C dates obtained (Table 1) do not reveal any reworking of sediments and a fitting curve extrapolates a $R^2=0.9884$. The time span represented by the core covers the last ~ 7000 BP. The calibrated dates yield an overall sedimentation rate of $0.1176 \text{ cm yr}^{-1}$, with a bottom date at 6870 ± 122 cal. BP (Figure 3a). Using the calibrated dates, we have calculated rates of sediment accumulation at each dated depth in the core, yielding a mean sedimentation rate of $0.0182 \text{ cm yr}^{-1}$. The resulting graph shows little variation in the sedimentation rate along the full length of the core (Figure 3b).

Sedimentology

Sediments generally showed a polymodal grain-size distribution and were ‘moderately well sorted’ to ‘very poorly sorted’ (Blott and Pye, 2001; Krumbein and Pettijohn, 1938) (Figure 4). We observed a dominant silt fraction ($>60\%$), a clay fraction ($<20\%$), and a sand fraction (mostly $<10\%$). With the exception of a peak of 20% between 540 and 510 cm (5200–4800 cal. BP), the clay fraction disappeared between ~ 700 and 280 cm (~ 6000 –2800 cal. BP). In the same interval, mean and median reached their highest values, and the sorting is lowest. Moreover, the mean is much higher than the median, illustrating a more coarsely skewed distribution (i.e. more fine than coarse material) (Bouchard et al., 2011). Mean and median grain sizes were correlated with silt and clay percentages (the finer particles), whereas sorting profiles coincided with sand percentages (the coarser particles) (Bouchard et al., 2011).

Once corrected for the porosity, the volumetric magnetic susceptibility showed a general decreasing trend from bottom to top, from ~ 840 to ~ 240 SI. Some peaks appear at regular intervals along the core; these are artifacts from the ends of the 1-m-long sections of the piston core (Figure 4). Between the base of the core and ~ 730 cm downcore, the decrease is faster (~ 240 SI), while between ~ 730 cm and the top of the core, the volumetric magnetic susceptibility decrease is slow, remaining mostly between ~ 400 and ~ 600 SI. In the uppermost ~ 5 cm, the volumetric magnetic susceptibility decreased from ~ 400 to ~ 240 SI (Figure 4).

Palynomorph fluxes

Using the sedimentation rates (cm yr^{-1}) calculated and extrapolated from the AMS- ^{14}C analyses and palynomorph concentration

(specimen cm^{-3}), we were able to calculate fluxes of the five counted palynomorphs in specimens $\text{cm}^{-2}\text{yr}^{-1}$ (Figure 5). All palynomorphs show similar trends throughout the length of the core and display a series of oscillations between high and low flux values (Figure 5). High values of all palynomorphs occur between ~ 7000 – 5200 , ~ 3600 – 2100 , and ~ 1000 – 700 cal. BP. During the first interval, pre-Quaternary palynomorphs reach their maximum value at $285 \text{ grains cm}^{-2}\text{yr}^{-1}$. Between ~ 1000 and 700 cal. BP, all palynomorphs, with the exception of pre-Quaternary palynomorphs, reach their maximum values: dinocyst fluxes $1000 \text{ grains cm}^{-2}\text{yr}^{-1}$, terrestrial palynomorphs $3000 \text{ grains cm}^{-2}\text{yr}^{-1}$, *Halo-dinium* $120 \text{ grains cm}^{-2}\text{yr}^{-1}$, and foraminifer linings $270 \text{ grains cm}^{-2}\text{yr}^{-1}$. Minimum values of all palynomorphs occur between 5200 and 3600 cal. BP, and a decreasing trend is observed from 700 cal. BP until today.

Pollen and spore assemblages

The core assemblages portray a type of vegetation linked to tundra and forest tundra landscapes (Fallu et al., 2002; Lamb, 1984; Roberts et al., 2006), with a strong abundance of shrub-like tree pollen (*Betula* sp. and *A. crispa*), a relatively high abundance of coniferous tree pollen (*Pinus* sp. and *Picea* sp.) with some herbs pollen (Cyperaceae, Chenopodiaceae, Ericaceae, Asteraceae, *Epilobium latifolium*) and spores (Figure 6).

Five pollen zones can be distinguished. Zone A, at the bottom of the core between 7000 and 6000 cal. BP, is characterized by the lowest relative abundances of *A. crispa* (on average 38%) and shrub-like tree pollen grains (on average 50%) and the highest abundances of herbs pollen (on average 27%) of the whole core. From 6500 to 6000 cal. BP, there is a notable increase in *A. crispa* pollen abundance (+20%) concomitant with a decrease in herbs pollen grains (–15%).

Zone B, between 6000 and 4000 cal. BP, is mainly characterized by the maximum abundance of *A. crispa* (on average 63%) and the dominance of the shrub-like tree pollen (on average 71%). We also observed a drop of the abundance of herbs pollen to its present proportions (on average between 9% and 11%).

Zone C, between 4000 and 2000 cal. BP, is characterized by an increase in the relative abundance of coniferous tree pollen (+5%), especially *Picea* sp. We also observed an equivalent decrease of the relative abundance of the shrub-like tree pollen (–6%), especially *A. crispa*.

Zone D, between 2000–1000 cal. BP, is characterized by the highest abundance of coniferous tree pollen (on average 28%) and another drop of 10% in the relative abundance of the shrub-like tree pollen.

Zone E (the last 1000 cal. BP) is characterized by the highest abundance of *Betula* sp. (on average 22%) and the dominance of shrub-like tree pollen (on average 71%). The relative abundance of the coniferous tree pollen decreased to the level of zone A.

Dinocyst assemblages

The sediment core is characterized by the dominance of dinocysts belonging to heterotrophic taxa of dinoflagellates (*Islandinium minutum* s.l., *Brigantedinium* sp., *Echinidinium karaense*, and *Polykrikos* Arctic Morphotypes I and II). Only one dinocyst species associated with autotrophic dinoflagellate taxa is present (*Pentapharsodinium dalei*). It has a high abundance (on average 55%) between 7000 and 3400 cal. BP and disappears around ~ 2600 cal. BP (Figure 7).

We identified five main dinocyst zones. Zone I, between 7000 and 6200 cal. BP, is characterized by the dominance of heterotrophic (on average 83%) over autotrophic (on average 16%) taxa. In this interval, we observe the concurrent increase of *P. dalei* (on average +20%) and decrease of *I. minutum* s.l. and *Brigantedinium* sp. (on average –20%).

PC-NACHVAK 602

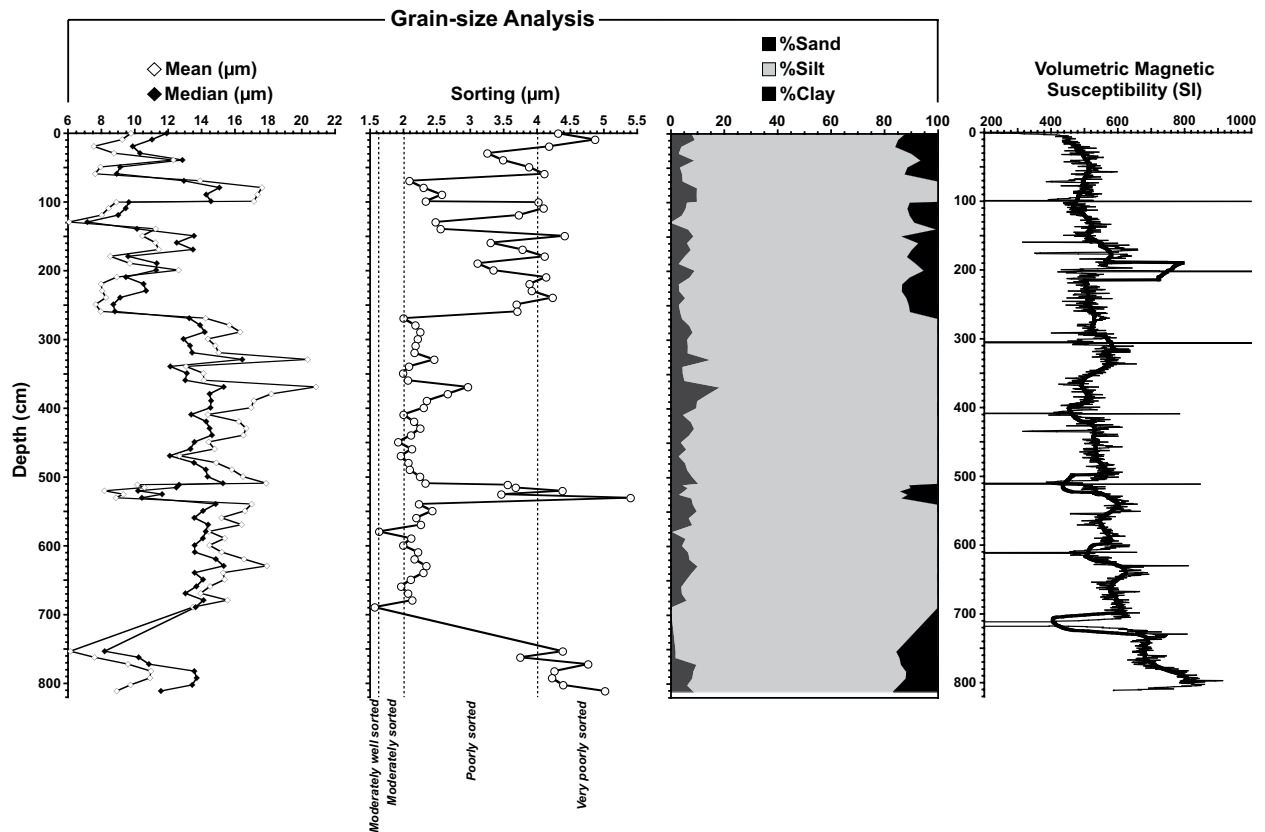


Figure 4. Sedimentological analyses of the core represented on a depth scale (cm). From left to right, grain-size analysis (mean, median and sorting (μm)); percentages of silt, sand, and clay; and volumetric magnetic susceptibility corrected for fractional porosity (SI).

PC-NACHVAK 602

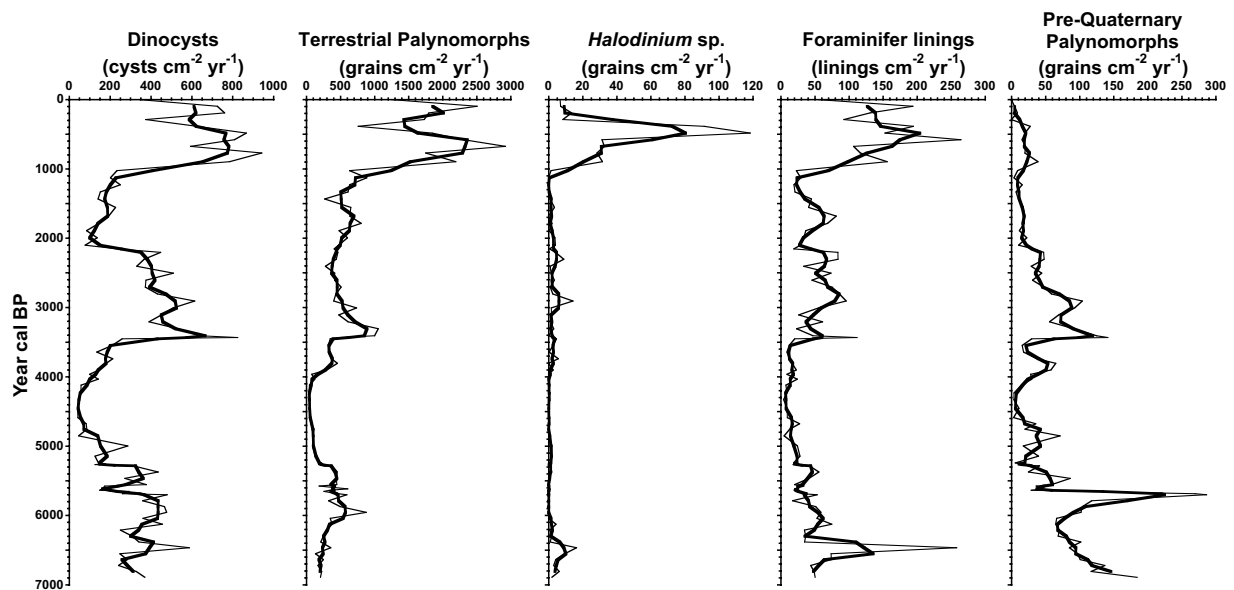


Figure 5. Fluxes of the five types of palynomorphs counted, according to time (cal. yr BP): dinocyst ($\text{cysts cm}^{-2}\text{yr}^{-1}$), terrestrial palynomorphs ($\text{grains cm}^{-2}\text{yr}^{-1}$), *Halodinium* sp. ($\text{grains cm}^{-2}\text{yr}^{-1}$), foraminifer linings ($\text{linings cm}^{-2}\text{yr}^{-1}$), and pre-Quaternary palynomorphs ($\text{grains cm}^{-2}\text{yr}^{-1}$). For each curve, the black thick line is a smooth of three values.

Zone II, between 6200 and 5000 cal. BP, is characterized by the highest abundance of *P. dalei* (on average 42%) and the lowest abundance of heterotrophic taxa (on average 58%).

Zone III, between 5000 and 3200 cal. BP, is characterized by the steady decrease of *P. dalei* (on average -14%) and the concurrent increase of the heterotrophic taxa (on average $+13\%$).

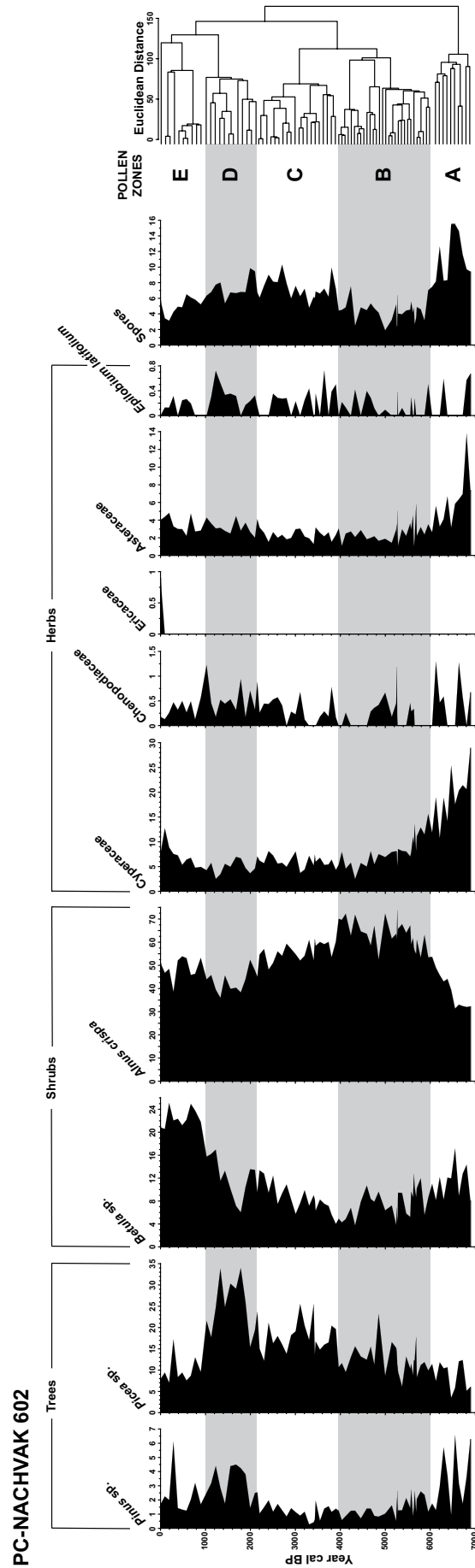


Figure 6. Pollen and spore zones identified based on the relative abundances (%) of major species observed in the core, according to time (cal. yr BP). Different shades of gray represent pollen zones obtained for each core using a cluster analysis.

PC-NACHVAK 602

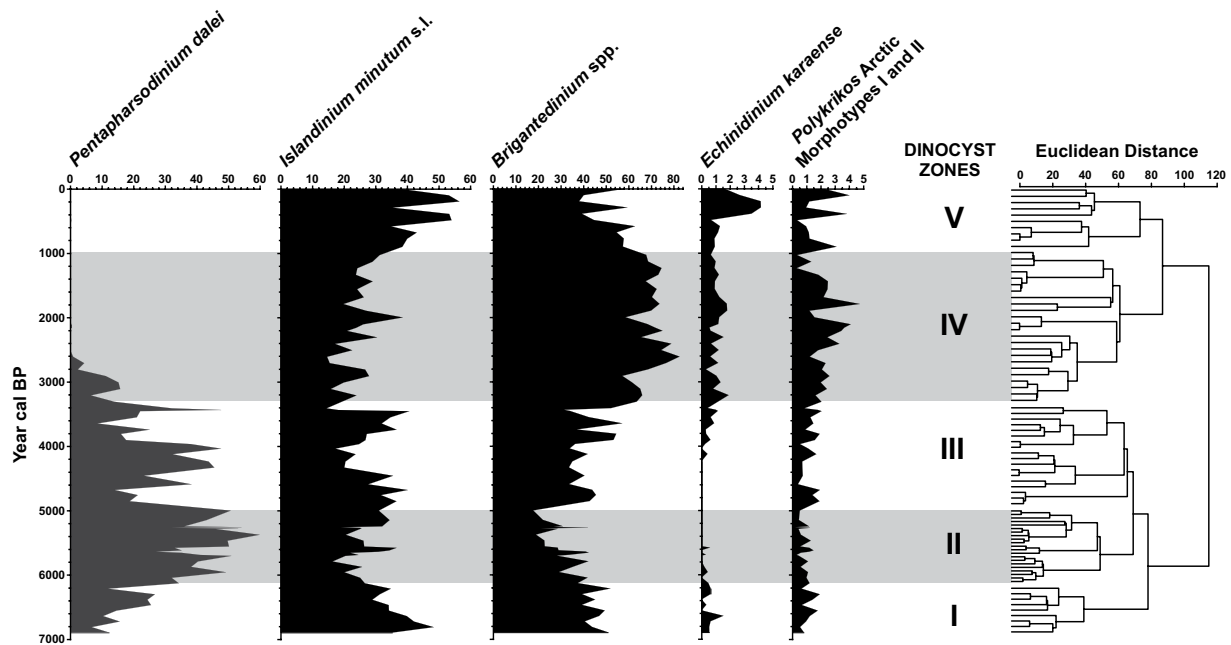


Figure 7. Dinocyst zones identified based on the relative abundances (%) of major species observed in the core, according to time (cal. yr BP). Different shades of gray represent pollen zones obtained for each core using a cluster analysis.

Zone IV, between 3200 and 1000 cal. BP, is characterized by the final disappearance of *P. dalei* at the beginning of the period (between 3310 and 2709 cal. BP) and the highest abundance of *Brigantedinium* sp. (on average 70%) and *Polykrikos* Arctic Morphotype I and II (on average 2%). This zone marks also the appearance of *E. karaense*.

Zone V, covering the last 1000 cal. BP, is characterized by the total dominance of heterotrophic taxa with the highest abundance of *I. minutum* s.l. (on average 45%) and *E. karaense* (on average 2%).

Paleoclimatic reconstructions

Pollen-based reconstructions. Using the modern analogs chosen for the pollen-based reconstructions, their origin and frequency of occurrence, we were able to document which types of biomes have influenced the region over the last ~7000 years. A graphic representation presents the average monthly temperature and precipitation for each pollen zone (Figure 8). Over the considered time period, the region was mostly influenced by 'Forest Tundra' biomes. The analogs chosen in pollen zone A originated mostly from sites in southern Labrador, suggesting less Arctic-like conditions. The strongest influence of the 'Boreal Forest' biomes was inferred for the period 6000–2000 cal. BP (zones B and C) associated with analogs from sites 'colder' (Mackenzie River Delta) and 'warmer' (Southern Labrador). The paleoclimatic reconstructions show dryer summers and slightly cooler winters. Zone D marks the decrease of the 'Boreal Forest' influence, associated with dryer and warmer winters and the wettest summers (Figure 8). The last ~1000 years show dominance of the 'Forest Tundra' influence over the region, with colder winters and dryer summers, and analogs mostly from 'colder' sites (Figure 8).

The three other reconstructed parameters show two types of trends. First, the annual precipitation and the mean temperature of the coldest month follow the same pattern of variation (Figure 9). A more or less important decrease between ~7000 and 6000 cal. BP (–200 mm and –2°C, respectively), followed by stable conditions between ~6000 and 2000 cal. BP (~320 mm and –27°C, respectively) that is only disrupted by two peaks at ~3800 cal. BP

(+200 mm and +3°C, respectively) and ~3100 cal. BP (+300 mm and +4°C, respectively) (Figure 9). Then an important increase occurs between ~2000 and 1000 cal. BP (+400 mm and +5°C, respectively), followed by a decrease in the last ~1000 years (–400 mm and –5°C, respectively) (Figure 9). The third reconstructed parameter, the mean temperature of the warmest month, shows a very different trend. First, we observe an increase between ~7000 and 6000 cal. BP (+4°C), followed by a very stable trend until the present day (around 10°C) (Figure 9).

Dinocyst-based reconstructions. The reconstructions of sea-surface parameters are generally in good agreement with the measured modern values of the environmental conditions (Richerol et al., 2012) (Figure 10). Between ~7000 and 5800 cal. BP, the reconstructed sea-surface temperatures for the warmest month of the year (August) declined by ~2°C, reaching temperatures comparable with the modern values. Meanwhile, the reconstructed sea-surface salinity for the warmest month decreased by ~6 units, whereas the reconstructed sea-ice cover duration and annual productivity increased by ~2 months yr⁻¹ and ~80 g C m⁻² yr⁻¹, respectively (Figure 10).

Between ~5800 and 3000 cal. BP, the reconstructed August temperatures remained stable around ~2°C, with the exception of a peak at ~3°C between ~3800 and 3300 cal. BP. The reconstructed salinity remained stable around ~22, with the exception of an abrupt decrease to 17 at ~4800 cal. BP and a peak at 28 between 3700 and 3000 cal. BP. The reconstructed sea-ice cover duration remained stable around ~8.6 months yr⁻¹, with the exception of a peak to ~9.4 months yr⁻¹ at ~4800 cal. BP and a decrease to ~7.6 months yr⁻¹ between 3800 and 3300 cal. BP. The reconstructed annual productivity remained stable around ~100 g C m⁻² yr⁻¹, with the exception of a decrease to ~60 g C m⁻² yr⁻¹ at ~5600 cal. BP and another one to ~70 g C m⁻² yr⁻¹ between ~4200 and 3500 cal. BP (Figure 10).

Between ~3000 and 1000 cal. BP, reconstructed temperatures generally showed an increasing trend (+1.2°C) with variations of the order of 1.4–3°C. In this interval, the salinity sharply increases from 19 to 29 (its modern value) within 300 years. The reconstructed sea-ice cover

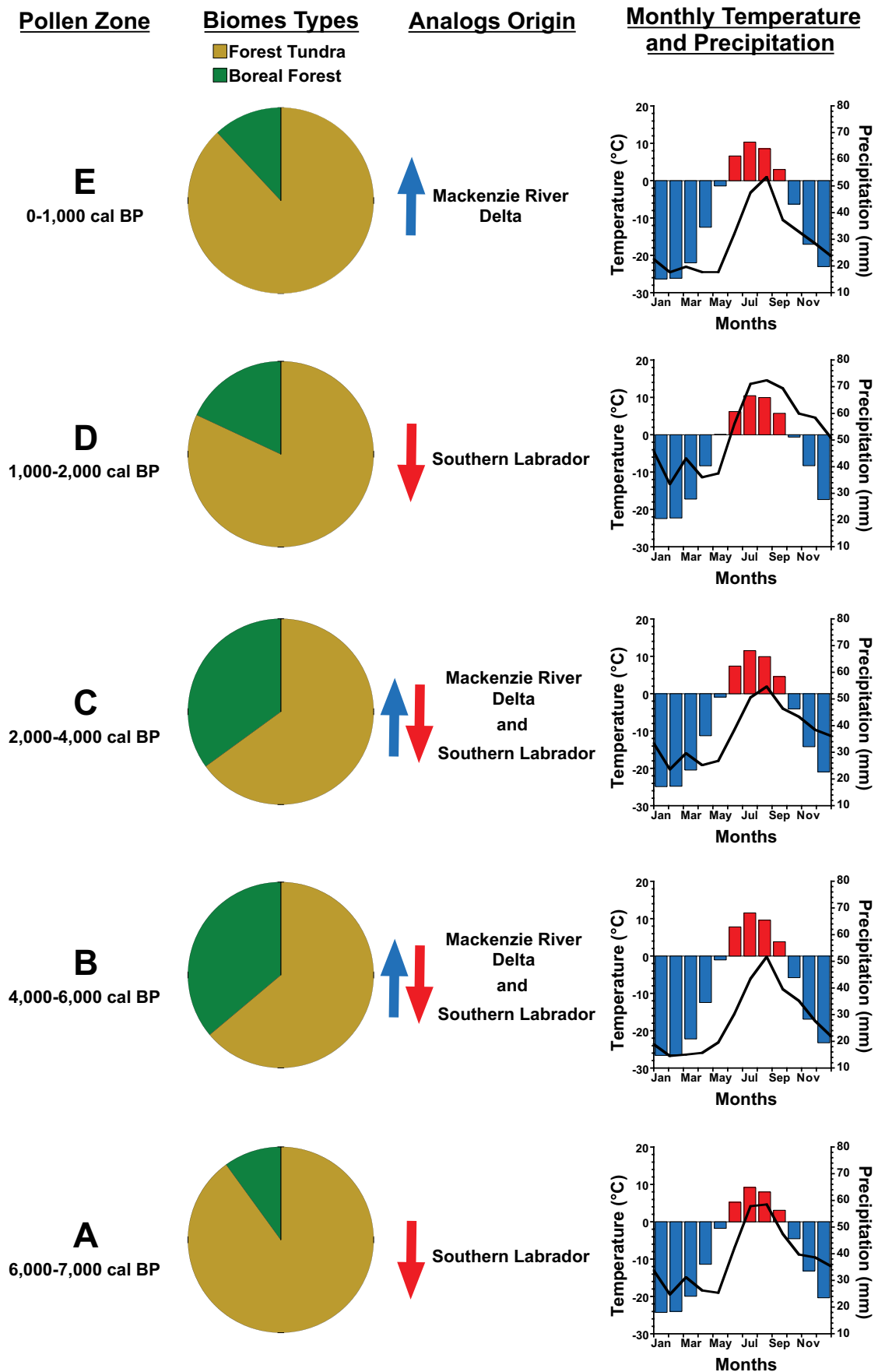


Figure 8. Graphic representation, according to the five pollen zones, of the biome types and origin of the analogs, and the mean reconstructed monthly temperature (°C – bars) and precipitation (mm – line). The blue upward pointing arrow illustrates the cold northern origin of the analogs and the red downward pointing arrow their warmer southern origin.

PC-NACHVAK 602

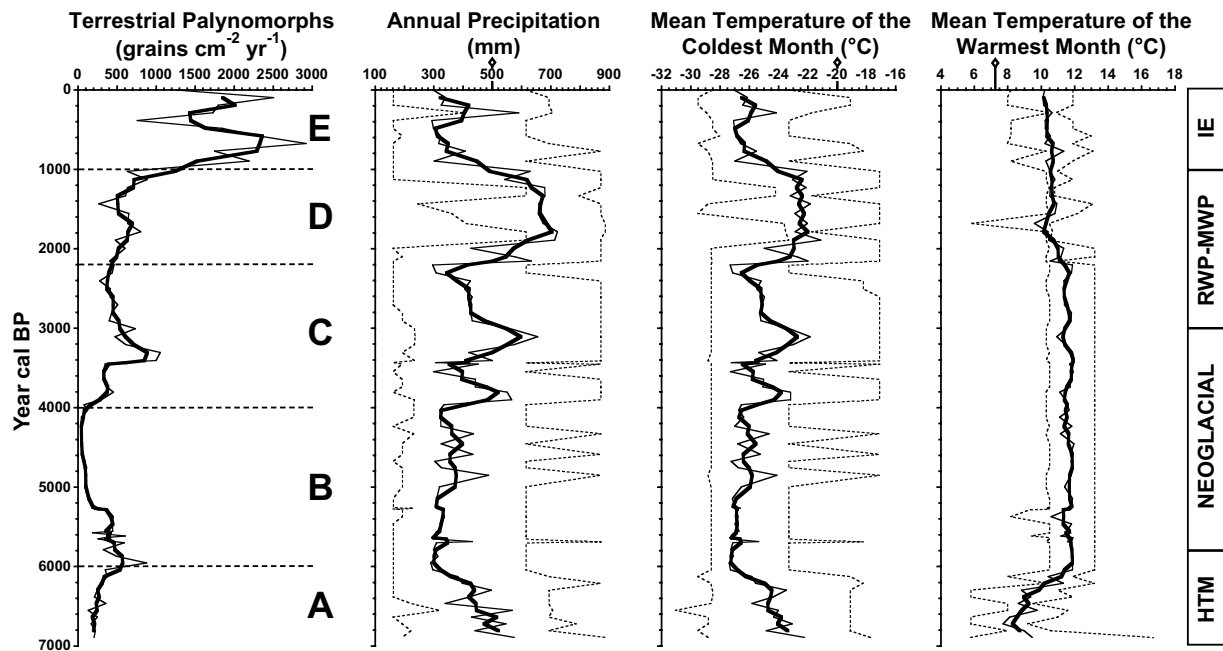


Figure 9. Evolution of terrestrial palynomorph fluxes (grains $\text{cm}^{-2} \text{yr}^{-1}$) in parallel with three reconstructed terrestrial parameters, according to time (cal. yr BP). Annual precipitation (mm) and mean temperature of the coldest and warmest months ($^{\circ}\text{C}$). For each curve, the black thick line is a smooth of three values. Horizontal black dotted lines on terrestrial palynomorphs fluxes represent major shifts in pollen zones. Thin dotted lines represent the confidence interval for each reconstructed parameter over time. For each parameter, the black empty diamonds on the x-axis represent modern values estimated from nearby meteorological stations (Cartwright 57°W and Goose A 60°W (Environment Canada)). HTM: Holocene Thermal Maximum; RWP: 'Roman Warm Period'; MWP: 'Medieval Warm Period'; IE: Industrial Era.

PC-NACHVAK 602

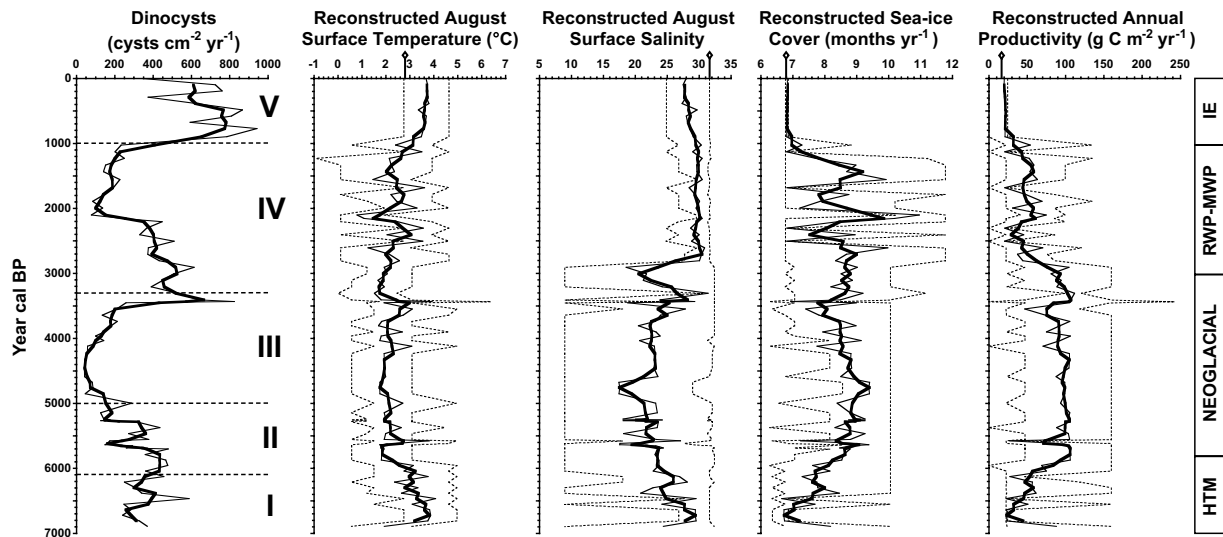


Figure 10. Evolution of dinocyst fluxes (cysts $\text{cm}^{-2} \text{yr}^{-1}$) in parallel with the four reconstructed oceanographic parameters, according to time (cal. yr BP). August sea-surface temperature ($^{\circ}\text{C}$), August sea-surface salinity, sea-ice cover duration (months yr^{-1}) and annual productivity ($\text{g C m}^{-2} \text{yr}^{-1}$). For each curve, the black thick line is a smooth of three values. Horizontal black dotted lines on dinocyst fluxes represent major shifts in dinocyst zones. Thin dotted lines represent the confidence interval for each reconstructed parameter over time. For each parameter, the black empty diamonds on the x-axis represent modern values. HTM: Holocene Thermal Maximum; RWP: 'Roman Warm Period'; MWP: 'Medieval Warm Period'; IE: Industrial Era.

duration showed a decreasing trend ($-2 \text{ months yr}^{-1}$) with important variations between ~ 10 and $\sim 7 \text{ months yr}^{-1}$. The reconstructed annual ocean productivity showed a decreasing trend of $60 \text{ g C m}^{-2} \text{ yr}^{-1}$ over

the same period (Figure 10). Over the last ~ 1000 years, the four reconstructed parameters remained relatively stable within the range of their modern instrumental values (Figure 10).

Discussion

This study describes features of the mid- to late-Holocene paleoclimate variability in the Labrador area, yet with slight deviations in the timing when compared with climate patterns reported from other Arctic and Sub-Arctic regions (Carlson et al., 2008; Peltier, 2004; Renssen et al., 2009). Based on the AMS-¹⁴C chronology, our paleorecord goes back in time to approximately ~7000 cal. BP corresponding to the end of the HTM in northern Labrador (Carlson et al., 2007; Kaplan and Wolfe, 2006; Kaufman et al., 2004) (Figure 3, Table 1).

End of HTM – 7000–5800 cal. BP

The higher volumetric magnetic susceptibility values recorded at the bottom of the core (810–720 cm; ~7000–6000 cal. BP) (Figure 4), together with the higher flux of pre-Quaternary palynomorphs during approximately the same period (~7000–5600 cal. BP) (Figure 5), suggest important detrital matter inputs, which can be associated with high meltwater influx from the remaining Laurentide Ice Sheet at the end of the last deglaciation (Carlson et al., 2008; Peltier, 2004; Sawada et al., 1999). During the same period, palynomorph fluxes show a peak in *Halodinium* sp. and foraminifer linings, which can be linked to freshwater inputs and an increase of benthic productivity (Figure 5). Considering the similar shifts in the fluxes of dinocysts and terrestrial palynomorphs all along the core, they portray synchronous variations in both terrestrial and marine habitats (Figure 5) (Sawada et al., 1999). Pollen zone A (7000–6000 cal. BP) shows a relatively high abundance of herbaceous taxa consistent with recently deglaciated landscapes and the recolonization by terrestrial vegetation (Figures 6 and 11) (Gajewski et al., 2000; Jessen et al., 2011; Richard, 1981; Ritchie, 1987; Viau and Gajewski, 2009). Dinocyst zone I (7000–6200 cal. BP) shows an increase in *P. dalei* and a decrease of *I. minutum* s.l., suggesting an increase in productivity, less turbidity, and a decrease of cold surface Arctic water intrusions (Figures 7 and 11). Levac et al. (2001), using dinocyst assemblages, have estimated the establishment of optimal conditions in Baffin Bay around 6400 BP and earlier. The climatic parameters reconstructed with the pollen assemblage show a decrease of the temperature of the coldest month associated with an increase of the warmest month (Figures 9 and 11). These events can be interpreted as a return to conditions with a stronger seasonality after a glacial era. The marine reconstructions suggest a slight cooling trend, together with a decrease in salinity and longer sea-ice duration (Figures 10 and 11) coherent with colder and dryer winter conditions on land (Figures 8, 9 and 11) and consistent with the end of deglaciation, input of freshwaters from the melting Laurentide Ice Sheet, and the onset of the next cooling period, the Neoglacial (Figures 9, 10 and 11) (Jessen et al., 2011; Levac, 2003; Levac and de Vernal, 1997; Nørgaard-Pedersen and Mikkelsen, 2009; Seidenkrantz et al., 2008; Solignac et al., 2011).

Neoglacial – 5800–3200 cal. BP

The onset of the Neoglacial was dated at ~3200 BP in southern and southwestern Greenland (Seidenkrantz et al., 2008), but at ~4800 BP in Ikersuaq fjord and Narsaq Sound in southern Greenland (Nørgaard-Pedersen and Mikkelsen, 2009). Previous studies showed colder sea-surface conditions North and South of Newfoundland between ~5700 and 4000 BP (Solignac et al., 2011), as well as North-West of Newfoundland in a bay under St Lawrence Gulf influence between ~6800 and 4000 BP (Levac, 2003), thereby suggesting an earlier onset of the Neoglacial. Rochon and de Vernal (1994) have associated *P. dalei* with the assemblage characteristic of the Labrador Sea and distinct from the assemblage of the Labrador shore and Labrador Current, similar to those inside the

Labrador fjords. Moreover, previous studies of benthic foraminifera and dinocyst assemblages around Hamilton Bank (southern Labrador coast) showed a weakening and slight warming of the cold Labrador Current between 8000 and 3500 BP (Fillon, 1976; Gajewski et al., 2000). The presence of *P. dalei* between ~7000–2600 cal. BP could be a signal of Labrador Sea water intrusions and of North Atlantic influences inside the fjord (Figures 7 and 11). The grain-size analysis shows a change in the sorting of the sediments between ~5200 and 4800 cal. BP (Figure 4), corresponding to a slight increase in pre-Quaternary palynomorph fluxes between 5300 and 4700 cal. BP (Figure 5). Pollen zone B (~6000–4000 cal. BP) shows an important abundance of *A. crispa*, associated with tundra-type vegetation and cold conditions (Figure 6). Although the modern pollen analogs show an increasing influence of warmer ‘Boreal Forest’ type biomes and occurrence of southern Labrador sites, the influence of colder ‘Forest Tundra’ type biomes is dominant (Figure 8). Richard (1981) and Gajewski et al. (2000) documented the growth of Forest Tundra in Nunavik (Northern Québec) over the same period, suggesting cold terrestrial conditions. Furthermore, palynological reconstructions by Gajewski et al. (2000) documented ‘polar desert and ice’ conditions in Northern Labrador around 6000 BP. Dinocyst zones II and III (~6000–3300 cal. BP) show a high abundance of *P. dalei* and an increase in the abundance of *I. minutum* s.l., suggesting high productivity and a higher input of cold Arctic waters, respectively (Figures 7 and 11). Our reconstructions also suggest colder conditions in Nunatsiavut starting around ~6000 cal. BP (Figures 9, 10 and 11). The grain-size analysis and the pre-Quaternary palynomorph fluxes seem to have registered an input of distant erosive material into the fjord. Previous studies from Agassiz Ice Cap (Ellesmere Island, Canada), Bonavista and Placentia bays (Newfoundland, Canada), and the Greenland Ice Sheet suggested the influence of the melting glaciers from the Canadian Arctic and Greenland (Fisher et al., 1995; Solignac et al., 2011; Vinther et al., 2009), which could explain the inferred low salinities and higher productivity associated with the presence of *P. dalei* between ~6000 and 3000 cal. BP (Figures 7, 10 and 11). Both pollen and dinocysts have recorded between ~5800 and 3200 cal. BP a cold period in Nunatsiavut (Figure 11). The paleoceanographic reconstructions suggest a growing cooling influence of Labrador Sea and North Atlantic waters over this period.

The sea-surface conditions northeast of Newfoundland have shown less severe conditions after ~4000 BP, which could reflect a general decrease in cold water export through the Labrador Current linked to colder conditions in the Arctic resulting in decreased ice melt (Solignac et al., 2011). Pollen zone C (~4000–2000 cal. BP) is similar to pollen zone B in terms of analogs (Figure 8) and shows an increase of *Picea* sp. and a decrease of *A. crispa* (Figure 6), suggesting more pollen transport from Boreal Forest and a slight warming of the terrestrial conditions. The pollen reconstructions for this period show two peaks of warmer and wetter conditions at 3800 and 3100 cal. BP (Figures 9 and 11). Dinocyst zone III (~5000–3300 cal. BP) shows a progressive disappearance of *P. dalei* and an increase of *I. minutum* s.l. and *Brigantedinium* sp. (Figures 7 and 11). The marine reconstructions for this period show cold and stable conditions with a slight warming trend until 3500 cal. BP when a peak in temperature appears (Figures 10 and 11). During this period, an important decrease in salinity is mirrored by an increase in sea-ice cover duration (Figures 10 and 11). The lower salinity could indirectly reflect the wetter continental conditions and increased input of freshwater into the fjord, while *Halodinium* sp. shows a slight increase during this period (Figure 5) and the pollen reconstructions reveal a slight increase in the mean monthly precipitation between pollen zones B and C (Figure 9). The resulting increased inputs of freshwater could also be responsible for the slight warming of the surface waters in the fjord.

'Roman Warm Period'–'Medieval Warm Period'–3200–1000 cal. BP

The paleoclimatic reconstructions obtained within the last 1000 years of pollen zone C (3200–2200 cal. BP) suggest terrestrial conditions more in line with the end of the Neoglacial than the 'Roman Warm Period'–'Medieval Warm Period' (RWP-MWP) (Figures 9 and 11). By comparing them to the paleoceanographic reconstructions, we observe a lag of 1000 years in the transition between both periods (Figure 11). The RWP-MWP seems to have begun later (around 2000 cal. BP) on land.

Pollen zone D (~2000–1000 cal. BP) shows the highest *Picea* sp. abundances (Figure 6). The modern pollen analogs came mostly from sites in southern Labrador, but show less influence from the 'Boreal Forest' type biome (Figure 8), suggesting an opening of the vegetation cover and a bias toward tree pollen. The paleoclimatic reconstructions show warmer and wetter conditions (Figures 9 and 11). This period corresponds to the second half of the dinocyst zone IV, with the total disappearance of *P. dalei* and the maximum abundance of *Brigantedinium* sp. (Figures 7 and 11). The marine reconstructions show fluctuations in the sea-surface temperature and sea-ice cover between ~3000 and 1400 cal. BP, and a stabilization of the salinity around its modern value. Between 1400 and 1000 cal. BP, the temperature increase and the sea-ice cover duration decrease to their modern values (Figures 10 and 11). This warming trend, recorded both by pollen and dinocysts between 3000 and 1000 cal. BP, is likely associated with both the RWP (~2000–1500 cal. BP) and the MWP (~1300–900 cal. BP) (Moros et al., 2012; Seidenkrantz et al., 2008; Solignac et al., 2011). The disappearance of *P. dalei* marks the end of the influence from the Labrador Sea and North Atlantic waters and is probably linked to the strengthening and cooling of the Labrador Current after 3000 BP, as recorded by fossil marine mollusks (Dyke et al., 1996).

IE – The last 1000 cal. BP

In the northern hemisphere, the last ~1000 years are usually marked by the colder climates of the 'Little Ice Age' (~500–200 BP) and the warming of the IE (the last ~200 years) (Moros et al., 2012; Nørgaard-Pedersen and Mikkelsen, 2009; Seidenkrantz et al., 2008; Solignac et al., 2011). Most of the research completed in the studied area does not show signs of the warming associated with the IE, but instead reveals very stable climatic conditions with even a slight cooling trend (Fallu et al., 2005; Laing et al., 2002; Richerol et al., 2014; Viau and Gajewski, 2009). In this study, pollen zone E reflects the establishment of the modern-day conditions of the fjords with a dominance of *Betula* sp. and *A. crispa* (Richerol et al., 2014), which are characteristic of shrub tundra vegetation and cooler conditions (Figures 6 and 11). Meanwhile, dinocyst zone V indicates the same scenario for the marine realm, with an increase in *I. minutum* s.l. and *E. karaense* usually associated with cold Arctic waters of the Labrador Current (Figures 7 and 11). The marine reconstructions show stable paleoceanographic conditions for the four parameters over the same period (Figures 10 and 11).

Conclusion

By combining geophysical and palynological data from a pristine fjord environment in northern Labrador, our study has provided new insights into the mid- to late-Holocene climate history of the Nunatsiavut region over the last ~7000 years. While Nachvak Fjord is mostly under Arctic Water influence, the presence of *P. dalei* illustrated a period of higher productivity and stronger influence from the Labrador Sea and North Atlantic inside the fjord between ~7000 and 3000 cal. BP.

The last ~1000 years of paleoceanographic history did not show any signs of the climate fluctuations usually associated with the cooling of the 'Little Ice Age' or the warming associated with the IE. The absence of *P. dalei* during this period illustrates a stronger influence of the cold Labrador Current in the fjord system, acting as a barrier against the influence of the Labrador Sea and North Atlantic waters. This entire period appears to have remained climatically stable in this region as documented in previous studies.

Our study shows that, despite the modern climate stability of the region with regards to the climate changes, its past climate history has nevertheless revealed the sensitivity of the fjord systems as recorders of important climatic shifts, both local and regional, in the North Atlantic region. It thus confirms the importance of the Nunatsiavut fjords as sentinels for a better understanding of the complete past climate variability of the Northern Hemisphere, for the purpose of rendering more reliable predictions of future climate trajectories for this region.

Acknowledgements

We wish to thank the officers and crew of the CCGS *Amundsen* for their help and support during the sampling at sea. We are also thankful, for their helpful comments, to Dr Francine McCarthy and Dr Frédérique Eynaud as reviewers, and Dr Fabienne Marret as Associate Editor for *The Holocene*.

Funding

This work was funded through grants from the Natural Sciences and Engineering Research Council of Canada (NSERC) and the Network of Centers of Excellence program *ArcticNet* awarded to Reinhard Pienitz and André Rochon, as well as through funding from the Nunatsiavut Government. The Center for Northern Studies (CEN) provided additional logistic support. Funding Sources Natural Sciences and Engineering Research Council of Canada, (Grant/Award Number: '170043')

References

- Arctic Climate Impact Assessment (ACIA) (2005) *International Arctic Science Committee (IASC)*. Cambridge: Cambridge University Press, 1020 pp.
- Arctic Monitoring and Assessment Programme (AMAP) (2011) *Snow, Water, Ice and Permafrost in the Arctic (SWIPA): Climate Change and the Cryosphere*. Oslo: AMAP, 538 pp.
- Barber DC, Dyke A, Hillaire-Marcel C et al. (1999) Forcing of the cold event of 8,200 years ago by catastrophic drainage of Laurentide lakes. *Nature* 400: 344–348.
- Barber DG (2010) Chapter 3.3 – Managing the largest Canadian watershed in a new climate: Land-Ocean interactions in sub-arctic Hudson Bay (Theme 3). In: Vincent WF, Lemay M and Barnard C (eds) *Impacts of Environmental Change in the Canadian Coastal Arctic: A Compendium of Research Conducted During ArcticNet Phase I (2004–2008)*, vol. 1. Québec City: ArcticNet Inc., pp. 43–53.
- Bell T and Josenhans H (1997) The seismic record of glaciation in Nachvak Fjord, Northern Labrador. In: Davies TA, Bell T, Cooper AK et al. (eds) *Glaciated Continental Margins: An Atlas of Acoustic Images*. London: Chapman & Hall, pp. 190–193.
- Bell T and Renouf MAP (2003) Prehistoric cultures, reconstructed coasts: Maritime Archaic Indian site distribution in Newfoundland. *World Archaeology* 35(3): 350–370.
- Bell T, Macpherson JB and Renouf MAP (2005a) Late prehistoric human impact on Bass Pond, Port au Choix. *Newfoundland and Labrador Studies* 20(1): 12.
- Bell T, Daly J, Batterson MJ et al. (2005b) Late Quaternary relative sea-level change on the West coast of Newfoundland. *Géographie Physique et Quaternaire* 59(2–3): 129–140.

- Bentley SJ and Kahlmeyer E (2012) Patterns and mechanisms of fluvial sediment flux and accumulation in two subarctic fjords: Nachvak and Saglek Fjords, Nunatsiavut, Canada. *Canadian Journal of Earth Sciences* 49: 1200–1215.
- Blott S and Pye K (2001) GRADISTAT: A grain size distribution and statistics package for the analysis of unconsolidated sediments. *Earth Surface Processes and Landforms* 26(11): 1237–1248.
- Bogus K, Mertens KN, Lauwaert J et al. (2014) Differences in the chemical composition of organic-walled dinoflagellate resting cysts from phototrophic and heterotrophic dinoflagellates. *Journal of Phycology* 50(2): 254–266.
- Borcard D, Gillet F and Legendre P (2011) *Numerical Ecology with R: Chapter 4 – Cluster Analysis*. In: Gentleman R, Hornik K and Parmigiani GG (eds) *Use R! Series*. New York: Springer, pp. 53–114.
- Bouchard F, Francus P, Pienitz R et al. (2011) Sedimentology and geochemistry of thermokarst ponds in discontinuous permafrost, subarctic Quebec, Canada. *Journal of Geophysical Research, Biogeosciences* 116(G2): 1–14.
- Brown T, Reimer K, Sheldon T et al. (2012) Chapter 10 – A first look at Nunatsiavut Kangidualuk ('fjord') ecosystems. In: Allard M and Lemay M (eds) *Nunavik and Nunatsiavut: From Science to Policy. An Integrated Regional Impact Study (IRIS) of Climate Change and Modernization*. Québec City: ArcticNet Inc., pp. 271–301.
- Carlson AE, Clark PU, Raisbeck GM et al. (2007) Rapid Holocene deglaciation of the Labrador sector of the Laurentide Ice Sheet. *Journal of Climate* 20: 5126–5133.
- Carlson AE, Legerand AN, Oppo DW et al. (2008) Rapid early Holocene deglaciation of the Laurentide ice sheet. *Nature Geoscience* 1: 620–624.
- De Blij HJ (ed.) (2005) *Atlas of North America*. New York: Oxford University Press.
- De Vernal A and Hillaire-Marcel C (1987) Paléoenvironnements du Wisconsinien moyen dans l'est du Canada par l'analyse palynologique et isotopique de sédiments océaniques et continentaux. *Revue de Géologie Dynamique et de Géographie Physique* 27: 119–130.
- De Vernal A, Bilodeau G, Hillaire-Marcel C et al. (1992) Quantitative assessment of carbonate dissolution in marine sediments from foraminifer linings vs. shell ratios; Davis Strait, Northwest North Atlantic. *Geology* 20(6): 527–530.
- Durantou L, Rochon A, Ledu D et al. (2012) Quantitative reconstruction of sea-surface conditions over the last ~150 yr in the Beaufort Sea based on dinoflagellate cyst assemblages: The role of large-scale atmospheric circulation patterns. *Biogeosciences* 9: 5391–5406.
- Dyke AS (2004) An outline of North American Deglaciation with emphasis on central and northern Canada. In: Ehlers J and Gibbard PL (eds) *Quaternary Glaciations – Extent and Chronology, Part II: North America*, vol. 2b. Amsterdam: Elsevier Science and Technology Books, pp. 373–424.
- Dyke AS, Dale JE and McNeely RN (1996) Marine molluscs as indicators of environmental change in glaciated North America and Greenland during the last 18,000 years. *Géographie Physique et Quaternaire* 50(2): 125–184.
- Engstrom DR and Hansen BCS (1985) Postglacial vegetational change and soil development in southeastern Labrador as inferred from pollen and chemical stratigraphy. *Canadian Journal of Botany* 63: 543–561.
- Fallu M-A, Allaire N and Pienitz R (2002) Distribution of freshwater diatoms in 64 Labrador (Canada) lakes: Species-environment relationship along latitudinal gradients and reconstruction models for water colour and alkalinity. *Canadian Journal of Fisheries and Aquatic Sciences* 59(2): 329–349.
- Fallu M-A, Pienitz R, Walker IR et al. (2005) Paleolimnology of a shrub-tundra lake and response of aquatic and terrestrial indicators to climatic change in arctic Québec, Canada. *Palaeogeography, Palaeoclimatology, Palaeoecology* 215: 183–203.
- Fensome RA and Williams GL (2004) *The Lentin and Williams Index of Fossil Dinoflagellates* (Contribution Series Number 42). Dallas, TX: American Association of Stratigraphic Palynologists Foundation.
- Fillon RH (1976) Hamilton Bank, Labrador Shelf: Postglacial sediment dynamics and paleoceanography. *Marine Geology* 20: 7–25.
- Fisher DA, Koerner RM and Reeh N (1995) Holocene climatic records from Agassiz Ice Cap, Ellesmere Island, NWT, Canada. *The Holocene* 5: 19–24.
- Fréchette B, de Vernal A, Guiot J et al. (2008) Methodological basis for quantitative reconstruction of air temperature and sunshine from pollen assemblages in Arctic Canada and Greenland. *Quaternary Science Reviews* 27: 1197–1216.
- Frère Marie-Victorin ÉC (1935) *Flore Laurentienne*. Montréal: Les Presses de l'Université de Montréal.
- Gajewski K, Vance R, Sawada M et al. (2000) The climate of North America and adjacent ocean waters ca. 6 ka. *Canadian Journal of Earth Sciences* 37: 661–681.
- Gibbard PL, Head MJ, Walker MJC et al. (2010) Formal ratification of the Quaternary System/Period and the Pleistocene Series/Epoch with a base at 2.58 Ma. *Journal of Quaternary Science* 25(2): 96–102.
- Gunn DE and Best AI (1998) A new automated and nondestructive system for high resolution multi-sensor core logging of open sediment cores. *Geo-Marine Letters* 18: 70–77.
- Hare FK and Hay JE (1974) The climate of Canada and Alaska. In: Bryson RA and Hare FK (eds) *World Survey of Climatology*, vol. II. Amsterdam: Elsevier Scientific Publishing Co, pp. 49–192.
- Head MJ, Harland R and Matthiessen J (2001) Cold marine indicators of the late Quaternary: The new dinoflagellate cyst genus *Islandinium* and related morphotypes. *Journal of Quaternary Science* 16: 621–636.
- Intergovernmental Panel on Climate Change (IPCC) (2013–2014) *World Meteorological Organization*. Cambridge: Cambridge University Press.
- Jessen CA, Solignac S, Nørgaard-Pedersen N et al. (2011) Exotic pollen as an indicator of variable atmospheric circulation over the Labrador Sea region during the mid to late Holocene. *Journal of Quaternary Science* 26(3): 286–296.
- Johnson WH, Hansel AK, Bettis EA III et al. (1997) Late Quaternary temporal and event classifications, Great Lakes Region, North America. *Quaternary Research* 47: 1–12.
- Kahlmeyer E (2009) *Comparison of the sedimentary record in three sub-arctic fjord systems in northern Labrador*. BSc thesis, Memorial University of Newfoundland, 79 pp.
- Kaplan MR and Wolfe AP (2006) Spatial and temporal variability of Holocene temperature in the North Atlantic region. *Quaternary Research* 65: 223–231.
- Karrow PF, Dreimanis A and Barnett PJ (2000) A proposed diachronic revision of Late Quaternary time-stratigraphic classification in the Eastern and Northern Great Lakes area. *Quaternary Research* 54: 1–12.
- Kaufman DS, Ager TA, Anderson NJ et al. (2004) Holocene thermal maximum in the western Arctic (0–180°W). *Quaternary Science Reviews* 23: 529–560.
- Kerwin MW, Overpeck JT, Webb RS et al. (2004) Pollen-based summer temperature reconstructions for the eastern Canadian boreal forest, subarctic, and Arctic. *Quaternary Science Reviews* 23: 1901–1924.
- Krumbein WC and Pettijohn FJ (1938) *Manual of Sedimentary Petrography*. New York: Appleton-Century-Crofts, 549 pp.

- Laing TE, Pienitz R and Payette S (2002) Evaluation of limnological responses to recent environmental change and caribou activity in the riviere George region, Northern Québec, Canada. *Arctic. Antarctic and Alpine Research* 34(4): 454–464.
- Lajeunesse P and St-Onge G (2008) The subglacial origin of the Lake Agassiz-Ojibway final outburst flood. *Nature Geoscience* 1: 184–188.
- Lamb HF (1984) Modern pollen spectra from Labrador and their use in reconstructing Holocene vegetational history. *Journal of Ecology* 72(1): 37–59.
- Lamb HF (1985) Palynological evidence for postglacial change in the position of tree limit in Labrador. *Ecological Monographs* 55(2): 241–258.
- Levac E (2003) Palynological records from Bay of Islands, Newfoundland: Direct correlation of Holocene paleoceanographic and climatic changes. *Palynology* 27: 135–154.
- Levac E and de Vernal A (1997) Postglacial changes of terrestrial and marine environments along the Labrador coast: Palynological evidence from cores 91-045-005 and 91-045-006, Cartwright Saddle. *Canadian Journal of Earth Sciences* 34: 1358–1365.
- Levac E, de Vernal A and Blake W Jr (2001) Sea-surface conditions in the northernmost Baffin Bay during the Holocene: Palynological evidence. *Journal of Quaternary Science* 16(4): 353–363.
- McAndrews JH, Berti AA and Norris G (1973) *Key to the Quaternary Pollen and Spores of the Great Lakes Region*. Toronto: Royal Ontario Museum, 65 pp.
- McCarthy FMG, Collins ES, McAndrews JH et al. (1995) A comparison of postglacial Arcellacean ('Thecamoebian') and pollen succession in Atlantic Canada, illustrating the potential of Arcellaceans for paleoclimatic reconstruction. *Journal of Paleontology* 69(5): 980–993.
- Macpherson JB (1982) Postglacial vegetational history of the eastern Avalon Peninsula, Newfoundland, and Holocene climatic change along the Eastern Canadian seaboard. *Géographie Physique et Quaternaire* 36: 175–196.
- Marcott SA, Shakun JD, Clark PU et al. (2013) A reconstruction of regional and global temperature for the past 11,300 years. *Science* 339: 1198–1201.
- Mertens KN, Verhoeven N, Verleye T et al. (2009) Determining the absolute abundance of dinoflagellate cysts in recent marine sediments: The *Lycopodium* marker-grain method put to the test. *Review of Palaeobotany and Palynology* 157: 238–252.
- Moros M, Jansen E, Oppo DW et al. (2012) Reconstruction of the late-Holocene changes in the Sub-Arctic Front position at the Reykjanes Ridge, north Atlantic. *The Holocene* 22(8): 877–886.
- Niessen F, Jarrard RD and Bucker C (1998) Log-based physical properties of the CRP-1 core, Ross Sea, Antarctica. *Terra Antarctica* 5(3): 299–310.
- Nørgaard-Pedersen N and Mikkelsen N (2009) 8000 year marine record of climate variability and fjord dynamics from Southern Greenland. *Marine Geology* 264: 177–189.
- Peltier W (2004) Global glacial isostasy and the surface of the ice-age Earth: The ICE-5G (VM2) model and GRACE. *Annual Review of Earth and Planetary Sciences* 32: 111–149.
- Radi T, Bonnet S, Cormier M-A et al. (2013) Operational taxonomy and (paleo-)autoecology of round, brown, spiny dinoflagellate cysts from the Quaternary of high northern latitudes. *Marine Micropaleontology* 98: 41–57.
- Reimer K and Biasutti M (2012) Chapter 1.7 – Nunatsiavut Nuluak: Baseline inventory and comparative assessment of three northern Labrador fjord-based marine ecosystems (project 3.7). In: Pienitz R, Lemay M, Michaud J et al. (eds) *Impacts of Environmental Change in the Canadian Coastal Arctic: A Compendium of Research Conducted During ArcticNet Phase I (2004–2008)*, vol. 2. Québec City: ArcticNet Inc., pp. 109–119.
- Reimer K, Brown TA and Reimer RW (2004) Discussion: Reporting and calibration of Post-Bomb 14C Data. *Radiocarbon* 46: 1299–1304.
- Reimer PJ, Bard E, Bayliss A et al. (2013) INTCAL13 and MARINE13 radiocarbon age calibration curves 0–50,000 years cal BP. *Radiocarbon* 55(4): 1869–1887.
- Renssen H, Seppä H, Heiri O et al. (2009) The spatial and temporal complexity of the Holocene thermal maximum. *Nature Geoscience* 2: 411–414.
- Richard PJH (1981) Paléophytogéographie postglaciaire en Ungava par l'analyse pollinique. *Paléo-Québec* 13: 153.
- Richard PJH (1995) Le couvert végétal du Québec-Labrador il y a 6 000 ans BP: Essai. *Géographie Physique et Quaternaire* 49(1): 117–140.
- Richerol T, Pienitz R and Rochon A (2012) Modern dinoflagellate cyst assemblages in surface sediments of Nunatsiavut fjords (Labrador, Canada). *Marine Micropaleontology* 88–89: 54–64.
- Richerol T, Pienitz R and Rochon A (2014) Recent anthropogenic and climatic history of Nunatsiavut fjords (Labrador, Canada). *Paleoceanography* 29(9): 869–892.
- Richerol T, Rochon A, Blasco S et al. (2008a) Distribution of dinoflagellate cysts in surface sediments of the Mackenzie Shelf and Amundsen Gulf, Beaufort Sea (Canada). *Journal of Marine Systems* 74: 825–839.
- Richerol T, Rochon A, Blasco S et al. (2008b) Evolution of paleo sea-surface conditions over the last 600 years in the Mackenzie Trough, Beaufort Sea (Canada). *Marine Micropaleontology* 68: 6–20.
- Ritchie JC (1987) *Postglacial Vegetation of Canada: 5. Eastern Canada – Fossil Record and Reconstruction*. Cambridge: Cambridge University Press.
- Roberts BA, Simon NPP and Deering KW (2006) The forest and woodlands of Labrador, Canada: Ecology, distribution and future management. *Ecological Research* 21: 868–880.
- Rochon A and de Vernal A (1994) Palynomorph distribution in recent sediments from the Labrador Sea. *Canadian Journal of Earth Sciences* 31: 115–127.
- Rochon A, de Vernal A, Turon J-L et al. (1999) *Distribution of Recent Dinoflagellate Cysts in Surface Sediments from the North Atlantic Ocean and Adjacent Seas in Relation to Sea-surface Parameters* (Contribution Series Number 35). Dallas, TX: American Association of Stratigraphic Palynologists Foundation, 152 pp.
- Rousseau C (1974) *Géographie floristique du Québec/Labrador – Distribution des principales espèces vasculaires* (Travaux et Documents du Centre d'Études Nordiques (CEN)). Québec: Les Presses de l'Université Laval.
- Saulnier-Talbot E and Pienitz R (2010) Postglacial chironomid assemblage succession in northernmost Ungava Peninsula, Canada. *Journal of Quaternary Science* 25(2): 203–213.
- Sawada M, Gajewski K, de Vernal A et al. (1999) Comparison of marine and terrestrial Holocene climatic reconstruction from northeastern North America. *The Holocene* 9(3): 267–277.
- Seidenkrantz M-S, Roncaglia L, Fischel A et al. (2008) Variable North Atlantic climate seesaw patterns documented by a late Holocene marine record from Disko Bugt, West Greenland. *Marine Micropaleontology* 68: 66–83.
- Shaw J, Gareau P and Courtney RC (2002) Palaeogeography of Atlantic Canada 13–0 kyr. *Quaternary Science Reviews* 21: 1861–1878.
- Shaw J, Piper DJW, Fader GBJ et al. (2006) A conceptual model of the deglaciation of Atlantic Canada. *Quaternary Science Reviews* 25: 2059–2081.

- Sheldon T and Bell T (2012) Chapter 4.6 – Understanding and responding to the effects of climate change and modernization in Nunatsiavut (Nunatsiavut Nuluak). In: ArcticNet (ed.) *ArcticNet Annual Research Compendium (2011–2012)*. Québec City: ArcticNet Inc., 18 pp.
- Sheldon T and Bell T (2013) Chapter 4.6 – Understanding and responding to the effects of climate change and modernization in Nunatsiavut. In: ArcticNet (ed.) *ArcticNet Annual Research Compendium (2012–2013)*. Québec City: ArcticNet Inc., 34 pp.
- Short SK and Nichols H (1977) Holocene pollen diagrams from subarctic Labrador-Ungava: Vegetational history and climatic change. *Arctic and Alpine Research* 9: 265–290.
- Smol JP, Wolfe AP, Birks HJB et al. (2005) Climate-driven regime shifts in the biological communities of arctic lakes. *Proceedings of the National Academy of Sciences of the United States of America* 102(12): 4397–4402.
- Solignac S, Seidenkrantz M-S, Jessen C et al. (2011) Late-Holocene sea-surface conditions offshore Newfoundland based on dinoflagellate cysts. *The Holocene* 21(4): 539–552.
- Stuiver M, Reimer PJ and Reimer RW (2005) CALIB 7.0. Available at: <http://calib.qub.ac.uk/calib/> (accessed 30 September 2013).
- Syverson KM and Colgan PM (2011) The Quaternary of Wisconsin: An updated review of stratigraphy, glacial history and landforms. In: Ehlers J, Gibbard PL and Hughes PD (eds) *Quaternary Glaciations – Extent and Chronology: A Closer Look* (Developments in Quaternary Science), vol. 15, chapter 42. Amsterdam: Elsevier, pp. 537–552.
- Ullah W, Beersing A, Blouin A et al. (1992) *Water Resources Atlas of Newfoundland*. St John's, NL: Water Resources Division, Department of Environment and Lands, Government of Newfoundland and Labrador, pp. ii–80.
- Viau AE and Gajewski K (2009) Reconstructing millennial-scale, regional paleoclimates of boreal Canada during the Holocene. *Journal of Climate* 22(2): 316–320.
- Vinther BM, Buchardt SL, Clausen HB et al. (2009) Holocene thinning of the Greenland ice sheet. *Nature* 461: 385–388.
- Whitmore J, Gajewski K, Sawada M et al. (2005) Modern pollen data from North America and Greenland for multi-scale paleoenvironmental applications. *Quaternary Science Reviews* 24: 1828–1848.
- Williams JW, Webb T III, Richard PH et al. (2000) Late Quaternary biomes of Canada and the eastern United States. *Journal of Biogeography* 27: 585–607.
- Zonneveld KAF and Brummer G-JA (2000) (Palaeo-)ecological significance, transport and preservation of organic-walled dinoflagellate cysts in the Somali Basin, NW Arabian Sea. *Deep-Sea Research II* 47: 2229–2256.
- Zonneveld KAF, Versteegh GJM and de Lange GJ (1997) Preservation of organic-walled dinoflagellate cysts in different oxygen regimes: A 10,000 years natural experiment. *Marine Micropaleontology* 29: 393–405.
- Zonneveld KAF, Versteegh GJM and de Lange GJ (2001) Palaeoproductivity and post-depositional aerobic organic matter decay reflected by dinoflagellate cyst assemblages of the Eastern Mediterranean S1 sapropel. *Marine Geology* 172: 181–195.